
Membranes and Bioenergetics:
**Molecular Structures Involved in L-type
Calcium Channel Inactivation: ROLE OF
THE CARBOXYL-TERMINAL REGION
ENCODED BY EXONS 40-42 IN α 1C
SUBUNIT IN THE KINETICS AND Ca^{2+}
DEPENDENCE OF INACTIVATION**

Nikolai M. Soldatov, Roger D. Zühlke,
Alexandre Bouron and Harald Reuter
J. Biol. Chem. 1997, 272:3560-3566.
doi: 10.1074/jbc.272.6.3560

Access the most updated version of this article at <http://www.jbc.org/content/272/6/3560>

Find articles, minireviews, Reflections and Classics on similar topics on the [JBC Affinity Sites](#).

Alerts:

- [When this article is cited](#)
- [When a correction for this article is posted](#)

[Click here](#) to choose from all of JBC's e-mail alerts

This article cites 44 references, 13 of which can be accessed free at
<http://www.jbc.org/content/272/6/3560.full.html#ref-list-1>

Molecular Structures Involved in L-type Calcium Channel Inactivation

ROLE OF THE CARBOXYL-TERMINAL REGION ENCODED BY EXONS 40–42 IN α_{1C} SUBUNIT IN THE KINETICS AND Ca^{2+} DEPENDENCE OF INACTIVATION*

(Received for publication, September 10, 1996, and in revised form, November 14, 1996)

Nikolai M. Soldatov^{‡§}, Roger D. Zühlke[‡], Alexandre Bouron, and Harald Reuter[¶]

From the Department of Pharmacology, University of Bern, CH-3010 Bern, Switzerland

The pore-forming α_{1C} subunit is the principal component of the voltage-sensitive L-type Ca^{2+} channel. It has a long cytoplasmic carboxyl-terminal tail playing a critical role in channel gating. The expression of α_{1C} subunits is characterized by alternative splicing, which generates its multiple isoforms. cDNA cloning points to a diversity of human hippocampus α_{1C} transcripts in the region of exons 40–43 that encode a part of the 662-amino acid carboxyl terminus. We compared electrophysiological properties of the well defined 2138-amino acid $\alpha_{1C,77}$ channel isoform with two splice variants, $\alpha_{1C,72}$ and $\alpha_{1C,86}$. They contain alterations in the carboxyl terminus due to alternative splicing of exons 40–42. The 2157-amino acid $\alpha_{1C,72}$ isoform contains an insertion of 19 amino acids at position 1575. The 2139-amino acid $\alpha_{1C,86}$ has 80 amino acids replaced in positions 1572–1651 of $\alpha_{1C,77}$ by a non-identical sequence of 81 amino acids. When expressed in *Xenopus* oocytes, all three splice variants retained high sensitivity toward dihydropyridine blockers but showed large differences in gating properties. Unlike $\alpha_{1C,77}$ and $\alpha_{1C,72}$, Ba^{2+} currents (I_{Ba}) through $\alpha_{1C,86}$ inactivated 8–10 times faster at +20 mV, and its inactivation rate was strongly voltage-dependent. Compared to $\alpha_{1C,77}$, the inactivation curves of I_{Ba} through $\alpha_{1C,86}$ and $\alpha_{1C,72}$ channels were shifted toward more negative voltages by 11 and 6 mV, respectively. Unlike $\alpha_{1C,77}$ and $\alpha_{1C,72}$, the $\alpha_{1C,86}$ channel lacks a Ca^{2+} -dependent component of inactivation. Thus the segment 1572–1651 of the cytoplasmic tail of α_{1C} is critical for the kinetics as well as for the Ca^{2+} and voltage dependence of L-type Ca^{2+} channel gating.

charge carrier. Inactivation is usually greatly accelerated if Ba^{2+} is replaced by Ca^{2+} (2). The channels are also designated as L-type and are multisubunit proteins composed of the pore-forming α_{1C} subunit, which contains high affinity binding sites for DHPs (3–7), and of the auxiliary β and $\alpha_2\delta$ subunits (8, 9). Analysis of the hydrophobicity profile of α_{1C} indicates four repetitive motifs of similarity (I–IV), each composed of six transmembrane segments (S1–S6) (10). Both, the short amino-terminal tail encoded by exons 1 and 2, and the long carboxyl-terminal tail encoded by exons 38–50 of the human α_{1C} gene (11) are located in the cytoplasm.

Expression of α_{1C} is regulated through alternative splicing (12), which has primarily been detected in the membrane-spanning regions of the molecule. However, there is evidence that the carboxyl-terminal tail is also affected by alternative splicing. Two partial transcripts have been identified in a cDNA library of human hippocampus (11, 13). They show that exons 40–43 encoding the second quarter of the putative cytoplasmic tail of the α_{1C} molecule are subject to alternative splicing and may give rise to new α_{1C} splice variants in the brain.

The functional role of the carboxyl-terminal tail attracts much attention because of its potential involvement in channel gating. Removal of approximately 70% of the tail causes an increase in the opening probability of the rabbit cardiac α_{1C} channel (14). A similar deletion mutant of the human cardiac α_{1C} showed faster inactivation of the channel as compared to the wild-type channel (15). It has been concluded that this tail part of α_{1C} may serve as a critical component of the gating structure that influences inactivation properties of the channel (15).

In this report we describe two recombinant plasmids, pHLCC72 and pHLCC86, which contain alternative exons encoding parts of the carboxyl-terminal tails that are found in human hippocampus transcripts. After expression in *Xenopus* oocytes, we have analyzed electrophysiological properties of $\alpha_{1C,72}$ and $\alpha_{1C,86}$ channels and compared them with the reference $\alpha_{1C,77}$ channel (16). The results of our study show that amino acids encoded by exons 40–42 are important for the voltage dependence of activation and inactivation of the current through these channels, as well as for the kinetics and Ca^{2+} dependence of inactivation.

MATERIALS AND METHODS

Preparation of cDNAs Encoding α_{1C} Subunit Splice Variants—All splice variants were constructed within the frame of pHLCC77 (16) composed of exons 1–20, 22–30, 32–44, and 46–50 using the pBlue-script SK(–) vector (Stratagene) flanked at the 5'-end with *HindIII*/*BglII* and at the 3'-end with *BglII*/*BamHI* fragments of the *Xenopus* β -globin gene untranslated region sequences, respectively (17, 18). The recombinant plasmid pHLCC86 was prepared by replacing nucleotides 5104–5482 of pHLCC77, encoding exons 41 and 42, with the *BsaI*/*BglII*

DHP¹-sensitive Ca^{2+} channels of class C (1) are voltage-gated channels, which start to open at membrane voltages more positive than –40 mV and slowly inactivate if Ba^{2+} is the

* This work was supported by Grant 31-45093.95 from the Swiss National Science Foundation and a grant from the Sandoz Foundation. The costs of publication of this article were defrayed in part by the payment of page charges. This article must therefore be hereby marked "advertisement" in accordance with 18 U.S.C. Section 1734 solely to indicate this fact.

The nucleotide sequence(s) reported in this paper has been submitted to the GenBank™/EBI Data Bank with accession number(s) Z74996, Z34815, and Z34817.

[‡] These authors have contributed equally to this study.

[§] Present address: Dept. of Pharmacology, Georgetown Medical Center, Washington, DC 20007.

[¶] To whom correspondence should be addressed: Dept. of Pharmacology, University of Bern, Friedbühlstrasse 49, CH-3010 Bern, Switzerland. Tel.: 41-31-632-3281; Fax: 41-31-632-4992.

¹ The abbreviations used are: DHP, dihydropyridine; BAPTA, 1,2-bis(2-aminophenoxy)ethane-*N,N,N',N'*-tetraacetic acid Na_4 salt; nt, nucleotide(s); V_h , holding potential.

fragment of the coding frame of h54 cDNA, containing exons 40A and 40B and an upstream region of exon 43A (11). The recombinant plasmid pHLCC72 was constructed by substituting the *SfuI* (3726)/*ScaI* (5348) fragment of pHLCC77 with the respective fragment of h2.05 cDNA (11, 13), containing exon 41A with its 57-nt extension in the upstream direction. Nucleotide sequences of all obtained cDNAs were verified by the modified dideoxy termination method (19).

Template DNAs were linearized by digestion with *Bam*HI (pHLCC77 and pHLCC86) or *Not*I (pHLCC72), and capped transcripts were synthesized *in vitro* with T7 RNA polymerase using the mRNA cap kit (Stratagene).

Expression of Ca^{2+} Channels in *Xenopus* Oocytes—*Xenopus laevis* oocytes were defolliculated 1 day before injection (20). cRNA samples were dissolved in 5 mM HEPES, pH 6.8, and oocytes were injected with 50–100 nl of a mixture containing cRNAs (0.5 μ g/ μ l) for an α_{1C} splice variant, and for $\alpha_2\delta$ (21) and β_1 (22, 23) subunits in equimolar ratio. In some experiments β_{2A} or β_3 (24) subunits instead of β_1 were used. Injected oocytes were stored for 5–8 days in sterile Barth's medium supplemented with 100 units of penicillin/ml and 100 μ g of streptomycin/ml (Boehringer Mannheim, Rotkreuz, Switzerland). The medium was changed daily. Whole-cell Ba^{2+} currents (I_{Ba}) were recorded by a two-electrode voltage clamp method using an Axoclamp 2-A amplifier (Axon Instruments, Burlingame, CA) or a Warner Oocyte Clamp OC-725C (Warner Instrument Corp., Hamden, CT). Glass pipettes (Clark Electromedical Instruments, United Kingdom) were filled with 3 M CsCl and had resistances between 0.2 and 1 megohms. Throughout the experiments oocytes were continuously superfused at 5–15 ml/min. The Ba^{2+} bathing solution contained (in mM): $Ba(OH)_2$ 40, NaOH 50, KOH 1, HEPES 10 (pH 7.4 with methanesulfonic acid). Isradipine-containing solutions were prepared freshly from a stock solution.

In some experiments Ca^{2+} was used as charge carrier through the channels. One to 5 h prior to the recording of Ca^{2+} currents (I_{Ca}), oocytes were injected with 50 nl of a BAPTA solution containing 40 mM Na_2 -BAPTA and 10 mM HEPES (pH 7 with KOH). The bathing solution contained (in mM): $Ca(NO_3)_2$ 40, NaOH 50, KOH 1, HEPES 10 (pH 7.4 with methanesulfonic acid).

Voltage-clamp commands, current recordings and leak current subtraction were performed by means of the EPC software (Cambridge Electronic Design, Cambridge, UK). The EPC software analysis module, the KaleidaGraph software (Abelbeck, Reading, CA), and the FigP software (Biosoft, Ferguson, MO) were used for the data analysis. Statistical values are given as means \pm S.E. Membrane currents, filtered at 0.5–1 KHz and sampled at 2 KHz, were triggered by 0.25- or 1-s step depolarizations applied from V_h of -90 mV at a frequency of 0.033 Hz. All experiments were performed at room temperature (20–22 $^{\circ}$ C).

Inactivation characteristics of I_{Ba} through the three α_{1C} splice variants were measured with 2-s conditioning pre-pulses. An increase of the duration of conditioning pre-pulses from 2 s to 20 s produced, in all tested α_{1C} splice variants, an additional shift of the inactivation curves by 6 ± 2 mV toward more negative potentials without changes in their steepness, indicating that a steady state had not been reached with 2-s pre-pulses. However, the long pre-pulses were poorly tolerated by many oocytes; therefore, all inactivation curves reported in this paper have been obtained with a 2-s pre-pulse protocol and consequently are called "isochronic" inactivation curves.

To compare the sensitivities of α_{1C} splice variants toward DHPs, we have measured the fractional inhibition of I_{Ba} at $V_h = -90$ mV by different concentrations of (+)-isradipine ranging from 10 nM to 1 μ M. After application of isradipine, I_{Ba} was monitored at 30-s intervals until an equilibrium of the inhibition was reached. In these experiments endogenous, DHP-insensitive Ca^{2+} or Ba^{2+} currents (20) were not subtracted from recorded peak I_{Ba} amplitudes.

RESULTS

Structural Features of the Studied Splice Variants—We have compared electrophysiological properties of human α_{1C} splice variants: $\alpha_{1C,77}$ and two of its homologues, $\alpha_{1C,72}$ and $\alpha_{1C,86}$. Both homologues contain substitutions in the region of exons 40–42 encoding the second quarter of the putative cytoplasmic tail of α_{1C} (Fig. 1, upper panel, see diagram). The recombinant plasmids for $\alpha_{1C,72}$ (pHLCC72) and for $\alpha_{1C,86}$ (pHLCC86) were prepared by incorporation of partial cDNA clones (h2.05 and h54) into the nucleotide sequence of pHLCC77. These partial clones have been isolated earlier from the human hippocampus cDNA library (11, 13) and proved to be products of alternative

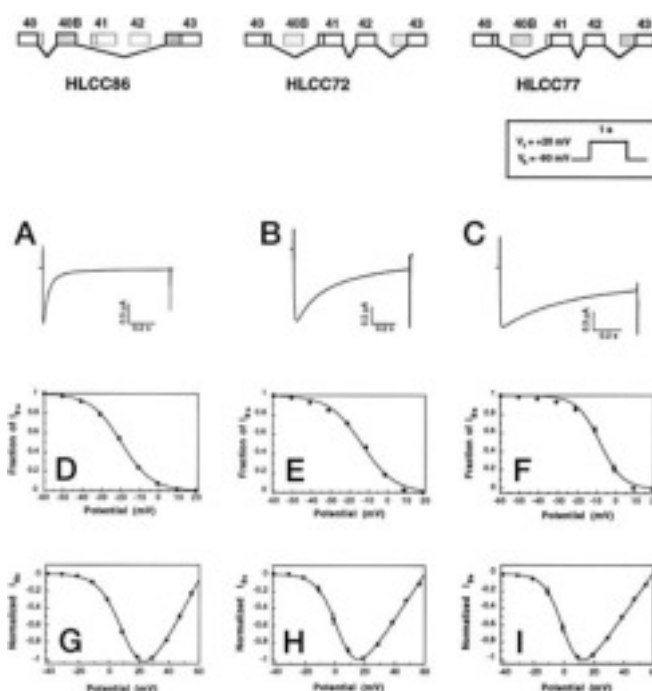


FIG. 1. Electrophysiological properties and location of variable parts of three α_{1C} splice variants. Schematic diagrams (upper panel) show the arrangement of exons, numbered according to Ref. 10, in three α_{1C} splice variants. Exons incorporated into the coding sequences are shown in bold lines. Deleted exons are shown in light lines. Shaded boxes point to exons found in human hippocampus transcripts. The inset shows the test pulse protocol for the traces of I_{Ba} through $\alpha_{1C,86}$ (A), $\alpha_{1C,72}$ (B), and $\alpha_{1C,77}$ (C). Averaged isochronic inactivation curves (12–16 experiments) of I_{Ba} through $\alpha_{1C,86}$ (D), $\alpha_{1C,72}$ (E), and $\alpha_{1C,77}$ (F) were obtained with 2-s conditioning pre-pulses (protocol not shown). The equation for fitting the data is given in Table II. G–I, averaged current-voltage relationships (10–18 experiments) of I_{Ba} through $\alpha_{1C,86}$, $\alpha_{1C,72}$, and $\alpha_{1C,77}$. Test pulses were applied at 30-s intervals. The equation for fitting the data is given in Table III. $V_h = -90$ mV. Pore-forming α_{1C} subunits were co-expressed with auxiliary β_1 and $\alpha_2\delta$ subunits at a 1:1:1 molar ratio.

splicing of one and the same α_{1C} gene (11). The nucleotide sequence of exon 41 in pHLCC72 is extended by 57 nt in the upstream direction and thus produces an insertion of 19 residues into the amino acid sequence of the $\alpha_{1C,72}$ channel at position 1575. In pHLCC86, 17 nt are deleted from the 3'-end of exon 40, the 102-nt exon 41 is replaced by the 118-nt exon 40B, and the 128-nt exon 42 is replaced by a 132-nt extension of exon 43 in the upward direction. Thus, 247 nt of the original pHLCC77 cDNA are replaced in pHLCC86 by 250 nt of a new coding sequence. At the amino acid level, this results in the replacement of 80 amino acid residues (1572–1651) of $\alpha_{1C,77}$ with 81 essentially non-identical amino acids in $\alpha_{1C,86}$ (Fig. 1). Amino acid alignments of the variable parts of the constructs have already been published (11). Because of this long stretch of non-identical amino acids, no mutagenesis has been attempted so far. All other parts of the recombinant channels studied in this work were unchanged.

None of the studied splice variants has yet been shown to be expressed in the brain. The $\alpha_{1C,86}$ channel is an "artificial" splice variant of the human α_{1C} . The partial cDNA clone h54 used to construct pHLCC86 shows further variability due to alternative splicing downstream of exon 43, which was not incorporated into the recombinant plasmid. A full-size transcript has not yet been cloned. Moreover, a fragment of an intron upstream of exon 40A indicates that h54 is not a part of a functional transcript but rather a product of post-transcriptional processing of the α_{1C} mRNA. However, both $\alpha_{1C,72}$ and $\alpha_{1C,86}$ showed a number of new characteristics pointing to an

TABLE I
Dependence of the kinetics of the I_{Ba} decay on the type of co-expressed $\alpha_{1\text{C}}$ and β subunits

Inactivation time constants, τ , of I_{Ba} were determined by test pulses to +20 mV from $V_h = -90$ mV. For $\alpha_{1\text{C},72}$ and $\alpha_{1\text{C},77}$ channels, τ was obtained from a single-exponential equation: $I(t) = I_\infty + I \exp(-t/\tau)$, where I_∞ is the steady state amplitude of the current and I is the amplitude of the initial current. The best fit for the current through the $\alpha_{1\text{C},86}$ channel was obtained by a bi-exponential equation: $I(t) = I_\infty + I_f \exp(-t/\tau_f) + I_s \exp(-t/\tau_s)$, where f and s stand for fast and slow components, respectively. I_{Ba} fractions refer to the respective contributions of fast and slow components to the total current through $\alpha_{1\text{C},86}$. In all cases the subunit composition of the analyzed channels was $\alpha_{1\text{C}}:\beta_1:\alpha_2\delta$ (1:1:1, moles). n = number of tested oocytes. *, $p < 0.05$ compared to the respective $\alpha_{1\text{C},77}$ channel (one-way ANOVA and Tukey test).

$\alpha_{1\text{C}}$ subunit (τ)	β subunit	τ	I_{Ba} fractions	n
		ms	%	
$\alpha_{1\text{C},77}$	β_1	484 ± 22		13
	$\beta_{2\text{A}}$	590 ± 62		5
	β_3	$1,341 \pm 144$		2
$\alpha_{1\text{C},72}$	β_1	$382 \pm 13^*$		14
	$\beta_{2\text{A}}$	721 ± 90		4
$\alpha_{1\text{C},86}$ (fast component)	β_1	$47.5 \pm 2.6^*$	84.6 ± 1.3	12
	$\beta_{2\text{A}}$	$71.3 \pm 6.7^*$	70.2 ± 7.7	2
	β_3	$55.8 \pm 3.9^*$	79.4 ± 2.6	2
$\alpha_{1\text{C},86}$ (slow component)	β_1	$210.5 \pm 10.2^*$	15.4 ± 1.3	12
	$\beta_{2\text{A}}$	$272.2 \pm 6.8^*$	29.8 ± 7.7	2
	β_3	$202.1 \pm 7.6^*$	20.6 ± 2.6	2

involvement of sequences encoded by exons 40–42 in important gating properties of the channel.

Differences between $\alpha_{1\text{C},77}$, $\alpha_{1\text{C},72}$, and $\alpha_{1\text{C},86}$ in Inactivation, Current-Voltage Relations, and Sensitivity to DHP Blockers—When cRNAs for $\alpha_{1\text{C},77}$, $\alpha_{1\text{C},72}$, or $\alpha_{1\text{C},86}$ were co-injected into *Xenopus* oocytes with cRNAs for auxiliary $\alpha_2\delta$ (21) and β_1 subunits (22, 23), they gave rise to functional Ca^{2+} channels with significantly different electrophysiological properties. Fig. 1 (A–C) show traces of I_{Ba} through splice variants of the pore-forming $\alpha_{1\text{C}}$ subunit recorded in response to depolarizing voltage clamp steps to +20 mV (1 s) from $V_h = -90$ mV. The inactivation kinetics of I_{Ba} through $\alpha_{1\text{C},86}$ was much faster than that through $\alpha_{1\text{C},77}$ and $\alpha_{1\text{C},72}$ channels. A direct comparison of time constants (τ) of inactivation obtained from exponential fits of the current traces is shown in Table I. In the case of $\alpha_{1\text{C},77}$ and $\alpha_{1\text{C},72}$, the kinetics of the I_{Ba} decay was fitted best by a single-exponential function. For $\alpha_{1\text{C},86}$ an exponential fit indicated two time constants, where the slow time constant, τ_s , was approximately 4 times that of the fast time constant, τ_f (Table I). Subtraction of the DHP-insensitive, endogenous I_{Ba} did not change significantly the absolute τ values. With β_1 co-expressed, the fast component of the inactivation phase of I_{Ba} through $\alpha_{1\text{C},86}$ comprised $84.6 \pm 1.3\%$ ($n = 12$) of the total current recorded with a 1-s pulse, while the slow component was $15.4 \pm 1.3\%$ ($n = 12$) (Table I). The slow component of I_{Ba} through $\alpha_{1\text{C},86}$ was still significantly faster than that through $\alpha_{1\text{C},77}$ or $\alpha_{1\text{C},72}$ channels (Table I).

The time constants of inactivation of I_{Ba} through $\alpha_{1\text{C},77}$, $\alpha_{1\text{C},72}$ and $\alpha_{1\text{C},86}$ showed different voltage dependences (Fig. 2A). In the case of $\alpha_{1\text{C},77}$, the time constant of inactivation of I_{Ba} decreased only slightly from $\tau_{(0)} = 455 \pm 38$ ms at 0 mV to $\tau_{(+40)} = 347 \pm 18$ ms at +40 mV ($n = 15$), i.e. by a factor of 1.3 (Fig. 2, B and C). Similarly, only a small voltage dependence of inactivation time constants was observed for $\alpha_{1\text{C},72}$. In the $\alpha_{1\text{C},86}$ channel, however, a more than 3.5-fold decrease of the fast inactivation time constant, from $\tau_{(0)} = 113 \pm 14$ ms ($n = 10$) to $\tau_{(+40)} = 29 \pm 1$ ms ($n = 14$) was measured (Fig. 2, B and C).

To characterize further the inactivation properties of the three splice variants of $\alpha_{1\text{C}}$, we examined the rate of recovery of I_{Ba} from inactivation. Fig. 3 shows the ratio of maximum amplitudes of I_{Ba} elicited by two consecutive test pulses with different intervals. The duration of the first pulse was 0.4, 2, or 3 s for $\alpha_{1\text{C},86}$, $\alpha_{1\text{C},72}$, and $\alpha_{1\text{C},77}$, respectively, a time required to reach 80–90% of inactivation of the currents through these channels. The second pulse lasted 400 ms. In Fig. 3 the ratios of I_{Ba} at pulse 2 divided by I_{Ba} at pulse 1 are plotted as function

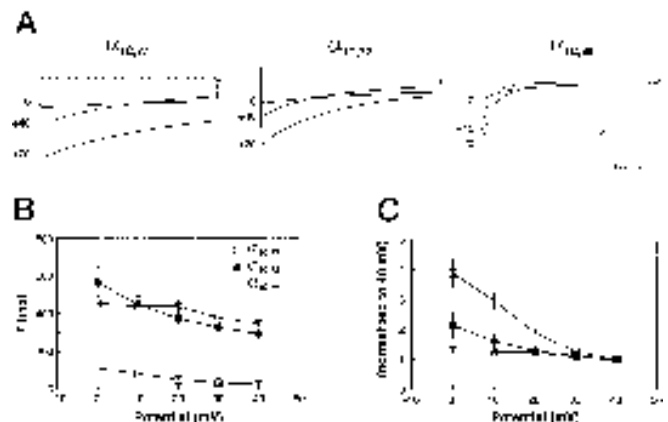


FIG. 2. Dependence of I_{Ba} inactivation kinetics on membrane potential. A, traces of I_{Ba} recorded at 0, +20, and +40 mV. The voltage dependence of the inactivation time constant (τ) was determined by fitting current traces of I_{Ba} in the range of 0 to +40 mV with exponential functions (B). Values of τ for $\alpha_{1\text{C},72}$ (●, $n = 10$) and $\alpha_{1\text{C},77}$ (○, $n = 15$) were determined by mono-exponential fitting. A bi-exponential approximation was used to obtain τ values for $\alpha_{1\text{C},86}$; only the fast component has been plotted in B and C (□, $n = 10$ –14). To illustrate differences in the voltage dependence of τ for the three $\alpha_{1\text{C}}$ splice variants, the values of τ at each potential were normalized with respect to τ at +40 mV (C). The subunit composition of the analyzed channels was $\alpha_{1\text{C}}:\beta_1:\alpha_2\delta$ (1:1:1, mol).

of the time intervals between the two pulses. This represents the fractional recovery of I_{Ba} from inactivation. Only the initial phase of recovery of I_{Ba} from inactivation could be fitted with a single-exponential function. This phase had approximately the same time constant for all three $\alpha_{1\text{C}}$ splice variants (Fig. 3). However, I_{Ba} through the $\alpha_{1\text{C},86}$ channel reached full recovery much faster than I_{Ba} through $\alpha_{1\text{C},72}$ and $\alpha_{1\text{C},77}$. At the 0.15-s interval between pulses, when 93 ± 1% ($n = 4$) of I_{Ba} through $\alpha_{1\text{C},86}$ had recovered, only 57 ± 2% of I_{Ba} through $\alpha_{1\text{C},72}$ and 56 ± 2% for $\alpha_{1\text{C},77}$ were available. With 16-s intervals between pulses, all measured I_{Ba} had almost completely recovered from inactivation.

As reported previously (21, 24), auxiliary β -subunits affect, among other properties, the kinetics of the Ca^{2+} channel current. We have found that β_1 , $\beta_{2\text{A}}$ or β_3 subunits, when co-expressed with $\alpha_2\delta$ and the splice variants of $\alpha_{1\text{C}}$ subunits, caused modulatory effects on the inactivation kinetics of I_{Ba} , which, however, were smaller than the differences between $\alpha_{1\text{C},86}$ and $\alpha_{1\text{C},77}$ or $\alpha_{1\text{C},72}$ (Table I).

Alternative splicing of exons 40–42 affects gating properties of the channel. Table II and Fig. 1 (D–F) show isochronic (2-s

pre-pulses) inactivation characteristics of I_{Ba} through the three α_{1C} splice variants. Isochronic inactivation curves were shifted toward negative potentials by 5 mV ($\alpha_{1C,72}$) and 11 mV ($\alpha_{1C,86}$) with respect to that of $\alpha_{1C,77}$ (Fig. 1, D–F; Table II, see $V_{0.5}$ values). The slopes of isochronic inactivation curves were less steep for $\alpha_{1C,86}$ and $\alpha_{1C,72}$ channels than for $\alpha_{1C,77}$ (Table II). Thus, cooperativity in the mechanism leading to inactivation of I_{Ba} may be different for $\alpha_{1C,86}$ and $\alpha_{1C,72}$ than for $\alpha_{1C,77}$.

Current-voltage relationships also point to differences in the voltage dependence of I_{Ba} through $\alpha_{1C,77}$ as compared to the other two splice variants (Table III, Fig. 1, G–I). In contrast to the negative shift of the inactivation curves of I_{Ba} through $\alpha_{1C,72}$ and $\alpha_{1C,86}$, their values for half-maximal activation were shifted toward more positive potentials by 6 mV and 11 mV, respectively (Fig. 1, G–I, and Table III). These data suggest that structural changes produced by alternative splicing of exons 40–42 in α_{1C} influence the voltage sensors of the channels for activation and inactivation in different ways. Since the reversal potentials of the current flowing through $\alpha_{1C,77}$, $\alpha_{1C,72}$, and $\alpha_{1C,86}$ channels are not significantly different (Table III), the pore region determining the selectivity of the channel is probably the same in the studied splice variants (25).

All three splice variants retain a high affinity for DHP block-

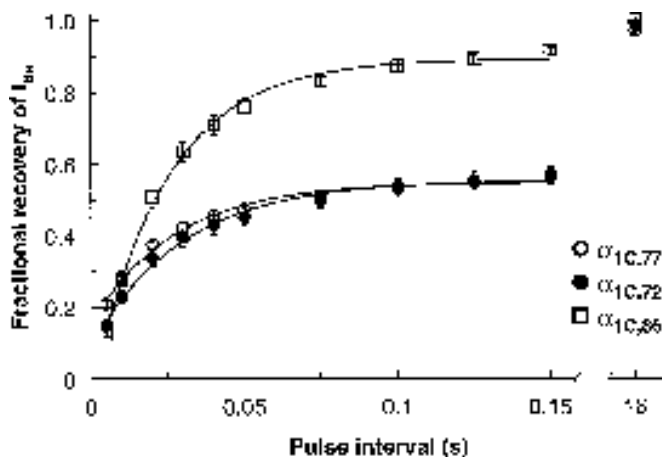


FIG. 3. Effect of α_{1C} subunit structures on the recovery of I_{Ba} from inactivation. Recovery of I_{Ba} through $\alpha_{1C,86}$ (\square), $\alpha_{1C,72}$ (\circ), and $\alpha_{1C,77}$ (\bullet) was measured with +20 mV pre-pulses of 0.4, 2, and 3 s in duration, respectively, and 0.4-s test pulses, both applied from $V_h = -90$ mV. The different pre-pulse durations for $\alpha_{1C,86}$, $\alpha_{1C,72}$, and $\alpha_{1C,77}$ were necessary to achieve 80–90% inactivation of I_{Ba} through each channel. Pre-pulses and test pulses were separated by increasing intervals. Smooth lines represent fits of the mean data by single exponentials with time constants $\tau = 27.2 \pm 0.9$ ms ($\alpha_{1C,77}$), $\tau = 30.0 \pm 1.6$ ms ($\alpha_{1C,72}$), $\tau = 24.0 \pm 2.1$ ms ($\alpha_{1C,86}$) ($n = 4$). The pore-forming α_{1C} subunit was co-expressed with auxiliary β_1 and $\alpha_2\delta$ subunits at equimolar ratio.

ers. When measured at $V_h = -90$ mV, the IC_{50} value for (+)-isradipine inhibition of I_{Ba} through $\alpha_{1C,77}$ is about 3.5 times higher than those for the other splice variants (Table III).

Differences between Splice Variants in Ca²⁺-dependent Inactivation—Besides voltage-dependent inactivation, many L-type Ca²⁺ channels exhibit Ca²⁺-dependent inactivation (2). This latter mode of inactivation has also been shown for heterologously expressed L-type Ca²⁺ channels (26–28). In view of the marked kinetic differences in inactivation between $\alpha_{1C,86}$, $\alpha_{1C,77}$, and $\alpha_{1C,72}$, we studied their respective Ca²⁺-dependent inactivation properties.

To buffer intracellular Ca²⁺ ions and to minimize contaminating Ca²⁺-dependent Cl⁻ currents, 50 nl of 40 mM BAPTA solution were injected into the oocytes prior to the recordings. The BAPTA injection did not affect properties of I_{Ba} . However, it could have reduced the response to Ca²⁺ of Ca²⁺-dependent inactivation, although Neely *et al.* (26) have shown that the time course of Ca²⁺-dependent inactivation remains virtually unchanged over a 20-fold range of buffering capacity. In Fig. 4, representative current traces recorded from oocytes during superfusion with 40 mM Ba²⁺ solution and after switching to 40 mM Ca²⁺ solution were superimposed. Ca²⁺ current (I_{Ca}) amplitudes were much smaller in all three channels than I_{Ba} amplitudes. This is consistent with a lower conductance for Ca²⁺ than for Ba²⁺ ions of L-type calcium channels (29). The reduction was less pronounced in $\alpha_{1C,86}$ compared to $\alpha_{1C,77}$ and $\alpha_{1C,72}$. The accelerated inactivation rate seen in $\alpha_{1C,77}$ and $\alpha_{1C,72}$, when Ca²⁺ was the charge carrier, was absent in $\alpha_{1C,86}$. This is illustrated in Fig. 4B, where peak I_{Ca} has been scaled up to the level of peak I_{Ba} . The scaling factors for $\alpha_{1C,77}$, $\alpha_{1C,72}$, and $\alpha_{1C,86}$ were 3.3, 2.9, and 1.8, respectively. In contrast to I_{Ba} inactivation kinetics of $\alpha_{1C,77}$ and $\alpha_{1C,72}$, I_{Ca} kinetics could not be fitted by a single exponential. With a bi-exponential fitting procedure, at +20 mV the fast time constants, τ_f , of I_{Ca} inactivation were 27.7 ± 1.9 ms ($n = 7$) and 34.4 ± 5.5 ms ($n = 4$) for $\alpha_{1C,77}$ and $\alpha_{1C,72}$, respectively. The I_{Ba} inactivation time constants were 398.7 ± 39.6 ms ($n = 7$) and 348.1 ± 22.1 ms ($n = 7$) in these experiments. Thus, an acceleration of the inactivation kinetics by a factor of 13 and 10 was observed if Ca²⁺ ions were the charge carriers through $\alpha_{1C,77}$ and $\alpha_{1C,72}$. By contrast, inactivation kinetics of $\alpha_{1C,86}$ were only slightly influenced by Ca²⁺ ions. The time constant, τ_f , observed at +20 mV in Ca²⁺ containing solution was 78.2 ± 8.0 ms ($n = 13$) compared to 59.0 ± 3.0 ms ($n = 10$) in Ba²⁺. The apparent slowing of the inactivation kinetics of $\alpha_{1C,86}$ by Ca²⁺ ions could be explained by a different surface potential with Ca²⁺ ions in the solution (30). This is also indicated by a slight shift toward more positive potentials of the current-voltage curve of all three calcium channel constructs when switching from Ba²⁺ to Ca²⁺ solution

TABLE II

Dependence of isochronic inactivation curves for I_{Ba} on α_{1C} and β subunits

Isochronic inactivation curves were measured using a two-step voltage clamp protocol. A 2-s conditioning pre-pulse was applied from $V_h = -90$ mV (10-mV increments up to +40 mV) followed by a 1-s test pulse to +20 mV. The intervals between each cycle were 30 s. Recorded peak current amplitudes were normalized to the maximum value determined in the range -60 to +20 mV. Isochronic inactivation curves were fitted by a Boltzmann function: $I_{Ba} = 1/(1 + \exp[(V - V_{0.5})/k])$, where V is the conditioning pre-pulse voltage, $V_{0.5}$ is the voltage at half-maximum of inactivation, and k is a slope factor. n = number of tested oocytes. *, $p < 0.05$ compared to the respective $\alpha_{1C,77}$ channel (one-way ANOVA and Tukey test).

α_{1C} subunit	β subunit	$V_{0.5}$ mV	Slope	n
$\alpha_{1C,77}$	β_1	-8.4 ± 1.1	5.7 ± 0.3	16
	β_{2A}	-9.7 ± 1.4	7.3 ± 0.4	5
	β_3	-9.1 ± 2.5	5.4 ± 0.1	3
$\alpha_{1C,72}$	β_1	$-13.6 \pm 0.7^*$	$8.6 \pm 0.3^*$	12
	β_{2A}	-11.8 ± 0.2	7.5 ± 0.3	2
$\alpha_{1C,86}$	β_1	$-19.9 \pm 0.5^*$	$7.8 \pm 0.2^*$	13
	β_{2A}	$-21.4 \pm 0.8^*$	7.7 ± 0.1	2
	β_3	-16.8 ± 0.9	$8.7 \pm 0.1^*$	2

TABLE III
Dependence of parameters of current-voltage relationships on α_{1C} and β subunits

I_{Ba} was measured with 30 s intervals between 1-s test pulses in the range of -40 to $+100$ mV (10-mV increments) applied from $V_h = -90$ mV. In all cases the subunit composition of the analyzed channels was $\alpha_{1C}:\beta:\alpha_2\delta$ (1:1:1, moles). I - V curves were fitted by $I_{\text{Ba}} = G_{\text{max}}(V - E_{\text{rev}})/[1 + \exp((V - V_{0.5})/k_{I,V})]$, where G_{max} = maximum conductance, E_{rev} = reversal potential, $V_{0.5}$ = voltage at 50% of I_{Ba} activation, and $k_{I,V}$ = slope factor. n = number of tested oocytes. Inhibition of I_{Ba} by isradipine (IC_{50}) has been measured at a test potential of $+20$ mV from a $V_h = -90$ mV without correction for endogenous DHP-insensitive I_{Ba} . *, $p < 0.05$ compared to the respective $\alpha_{1C,77}$ channel (one-way ANOVA and Tukey test).

Subunit		$I_{\text{Ba(max)}}$	E_{rev}	$V_{0.5}$	$k_{I,V}$	n	IC_{50} for isradipine (n)
α_{1C}	β						
		μA	mV	mV			nM
$\alpha_{1C,77}$	β_1	1.47 ± 0.14	59.8 ± 0.9	-0.3 ± 1.1	-5.6 ± 0.3	18	146.2 ± 12.2 (34)
	β_{2A}	0.58 ± 0.11	58.0 ± 0.7	2.2 ± 1.0	-7.0 ± 0.4	4	
	β_3	1.13 ± 0.02	59.3 ± 0.2	0.4 ± 1.1	-4.8 ± 0.2	2	
$\alpha_{1C,72}$	β_1	0.99 ± 0.12	60.3 ± 0.8	5.7 ± 2.0	-6.6 ± 0.3	12	39.8 ± 6.2 (10)*
	β_{2A}	1.23 ± 0.26	63.7 ± 2.3	5.9 ± 5.7	-6.5 ± 0.6	3	
$\alpha_{1C,86}$	β_1	$0.78 \pm 0.15^*$	62.5 ± 1.2	$11.5 \pm 1.8^*$	$-7.5 \pm 0.3^*$	10	37.7 ± 5.1 (9)*
	β_{2A}	1.04 ± 0.54	63.2 ± 4.9	8.0 ± 1.0	-7.1 ± 0.9	2	
	β_3	0.60 ± 0.03	63.0 ± 0.5	15.8 ± 0.7	$-9.0 \pm 0.1^*$	2	

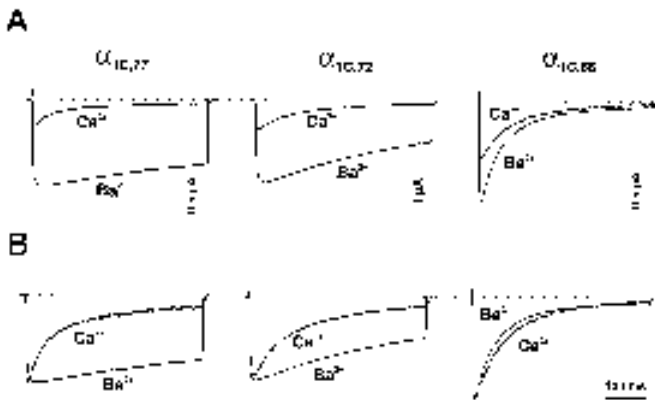


FIG. 4. Ca^{2+} -dependent inactivation occurs in $\alpha_{1C,72}$ and $\alpha_{1C,77}$ but not in $\alpha_{1C,86}$. I_{Ba} and I_{Ca} through $\alpha_{1C,77}$, $\alpha_{1C,72}$, and $\alpha_{1C,86}$ were recorded in *Xenopus* oocytes after injection of 50 nl of 40 mM BAPTA. Current traces were evoked by 400-ms depolarizing steps from $V_h = -90$ mV to $+20$ mV. The oocytes were superfused by a bath solution containing 40 mM Ba^{2+} or 40 mM Ca^{2+} . A, I_{Ba} and I_{Ca} recorded from the same oocyte expressing either $\alpha_{1C,77}$, $\alpha_{1C,72}$, or $\alpha_{1C,86}$. B, I_{Ca} traces from panel A normalized to peak I_{Ba} show that Ca^{2+} -dependent inactivation is present in $\alpha_{1C,77}$ and $\alpha_{1C,72}$ but absent in $\alpha_{1C,86}$. The individual α_{1C} subunits were co-expressed with auxiliary β_1 and $\alpha_2\delta$ subunits in an equimolar ratio.

(Fig. 5, B–D, filled triangles).

Ca^{2+} -induced inactivation is dependent upon the size of Ca^{2+} influx through the channel pore (2). This can be studied by applying a double-pulse protocol as shown in Fig. 5A (upper panel). The duration of the pre-pulse was 400 ms. A pulse interval of 50 ms was chosen, which was long enough to minimize incomplete recovery from partial inactivation during the pulse intervals. The test pulse was always to $+20$ mV and also lasted 400 ms. The interval between cycles was 30 s. Representative current traces for $\alpha_{1C,77}$ at the pre-pulse potentials -40 mV, $+20$ mV, and $+80$ mV for I_{Ba} (middle panel) and I_{Ca} (bottom panel) are shown in Fig. 5A. In Ba^{2+} solution, increasing pre-pulse potentials led to a persistent reduction (23.1%) of I_{Ba} through $\alpha_{1C,77}$ at the test pulse (Fig. 5, A and B). This is due to incomplete recovery from partial inactivation under these experimental conditions (data not shown). By contrast, with Ca^{2+} as charge carrier, the test pulse current (I_{TP}) exhibited a bell-shaped relation as a function of the pre-pulse potential (Fig. 5B). It was inversely related to the current amplitudes at the pre-pulse potentials (I_{PP}). The maximal current reduction of I_{TP} in Ca^{2+} solution was 53.5%, and became less with further depolarization during pre-pulses (Fig. 5, A and B). This is a strong indication for Ca^{2+} -dependent inactivation triggered by Ca^{2+} influx through $\alpha_{1C,77}$ channels. Application of the same

protocol to $\alpha_{1C,72}$ (Fig. 5C) resulted in a similar relationship between I_{PP} and I_{TP} as with $\alpha_{1C,77}$. The maximal current reductions were 15.9% in Ba^{2+} solution and 48.9% in Ca^{2+} solution. However, for $\alpha_{1C,86}$ (Fig. 5D) the relationships between I_{PP} and I_{TP} in Ba^{2+} and Ca^{2+} solutions (maximal current reductions were 22.8% and 24.3%, respectively) were almost identical and comparable to those obtained with $\alpha_{1C,77}$ and $\alpha_{1C,72}$ in Ba^{2+} solution. This provides further evidence that $\alpha_{1C,86}$ lacks Ca^{2+} -dependent inactivation.

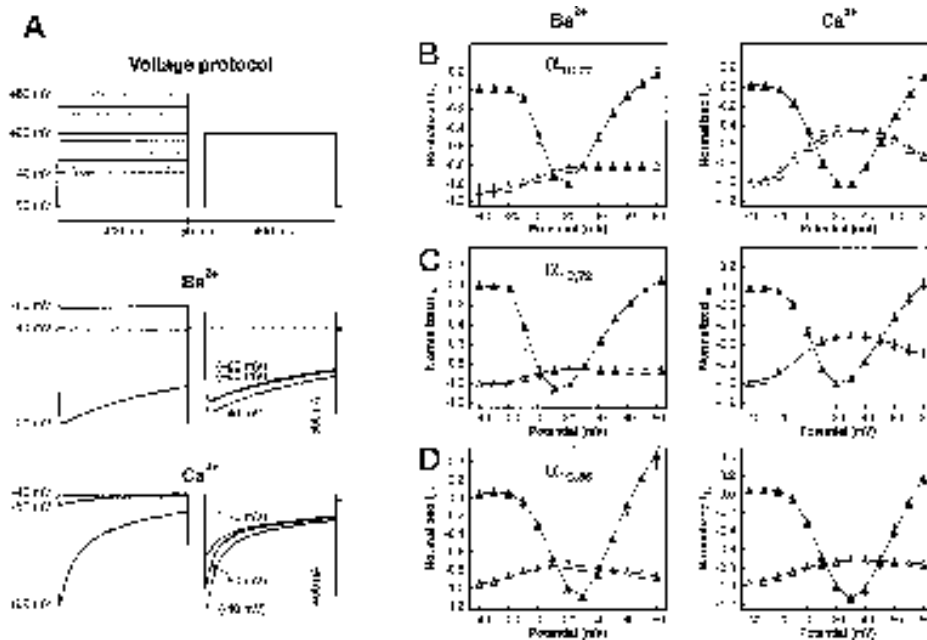
DISCUSSION

Alternative splicing of the α_1 subunit of voltage-dependent Ca^{2+} channels contributes to the structural diversity of these ion channels, but only little is known about its functional importance. It has been shown that alternative splicing of the gene encoding the α_{1C} subunit of L-type Ca^{2+} channels contributes to differences in the voltage dependence of the sensitivity toward DHPs (16) and to the DHP tissue selectivity (31). In this study we have investigated electrophysiologically three putative splice variants of the human class C L-type Ca^{2+} channel.

We show that a segment of 80 amino acids replaced in $\alpha_{1C,77}$ by a nonidentical sequence of 81 amino acids of $\alpha_{1C,86}$ in the second quarter of the 662-amino acid carboxyl-terminal tail (1572–1651) caused a 10-fold increase in the rate of inactivation, an 11-mV hyperpolarizing shift in the voltage dependence of inactivation, and elimination of Ca^{2+} -dependent inactivation, as well as an increase in the affinity of the channel to the DHP blocker (+)-isradipine. Some but not all of these effects were also partially visible in the $\alpha_{1C,72}$ channel. It is structurally identical to the reference 2138-amino acid $\alpha_{1C,77}$ channel, except for an insertion of 19 amino acids at position 1575 between sequences encoded by exons 40 and 41. There was a 5-mV hyperpolarizing shift of the voltage dependence of inactivation, the kinetics of inactivation of I_{Ba} through $\alpha_{1C,72}$ was only 20% faster than that through $\alpha_{1C,77}$ (Table I), and the DHP sensitivity of $\alpha_{1C,72}$ was the same as that of $\alpha_{1C,86}$ but about 4 times higher than that of $\alpha_{1C,77}$ (Table III).

Over the last few years, a multitude of studies have shed light on the molecular basis of Ca^{2+} channel inactivation. It has been suggested that voltage- and Ca^{2+} -dependent inactivation are regulated by distinct sites on the α_{1C} subunit (32). The structural determinants for voltage-dependent inactivation have been attributed to sequences near or in the S6 segments of domains I, III, and IV of the α_1 subunit (33, 34). Substituting as few as 9 amino acids from a rapidly inactivating class A Ca^{2+} channel near the transmembrane region IS6 for homologous residues in the α_{1C} subunit was sufficient to transform α_{1C} into a fast inactivating channel (33). More recently several studies have implicated carboxyl-terminal seg-

FIG. 5. Ca^{2+} -dependent inactivation in $\alpha_{1C,72}$ and $\alpha_{1C,77}$ requires Ca^{2+} influx. I_{Ba} and I_{Ca} in BAPTA-injected oocytes were elicited by a double-pulse voltage protocol (A). 400-ms depolarizing pre-pulses, applied in 10-mV increments from -90 mV to voltages ranging from -40 mV to +80 mV were followed by a 400-ms test pulse to +20 mV after a 50-ms pulse interval at -90 mV. Representative current traces through $\alpha_{1C,77}$ recorded from an oocyte superfused sequentially by 40 mM Ba^{2+} or 40 mM Ca^{2+} solutions are shown underneath the pulse protocol for pre-pulse potentials of -40, +20, and +80 mV. B-D, peak current amplitudes at pre-pulses (\blacktriangle) and test-pulses (\triangle) were normalized to the pre-pulse peak current at +20 mV and plotted versus the pre-pulse potential. The double-pulse protocol was applied to oocytes expressing $\alpha_{1C,77}$ (B, $n = 4$), $\alpha_{1C,72}$ (C, $n = 4$), and $\alpha_{1C,86}$ (D, $n = 7$) with 40 mM Ba^{2+} (left panel) and 40 mM Ca^{2+} (right panel) as charge carrier. The individual α_{1C} subunits were co-expressed with auxiliary β_1 and $\alpha_2\delta$ subunits in an equimolar ratio.



ments as being involved in voltage-dependent inactivation (15, 35).

The membrane-spanning regions, and consequently the voltage sensor in the S4 segments (36), are structurally identical in all three splice variants of α_{1C} studied in our work. The new amino acid sequences in the cytoplasmic carboxyl-terminal tail, encoded by alternative exons in $\alpha_{1C,72}$ and $\alpha_{1C,86}$, do not show hydrophobic stretches that would suggest their insertion into the plasma membrane. The differences in the voltage dependence of gating between $\alpha_{1C,77}$, $\alpha_{1C,72}$, and $\alpha_{1C,86}$ may, therefore, be due to an altered interaction of cytoplasmic amino acid sequences with the intramembrane voltage sensor in the S4 segments of the α_{1C} protein. For example, a direct interaction of the amino acids encoded by exons 40–42 with the cytoplasmic ends of the charged transmembrane segments S4 may affect the mobility of the charged regions in response to a change in the transmembrane electric field (37). This could influence the transitions between open and closed states of the channel depending on the conformational flexibility of the cytoplasmic polypeptide chains, which may be highest for the $\alpha_{1C,86}$ channel. However, we cannot rule out that the fast inactivation observed in $\alpha_{1C,86}$ may be due to some modulatory effect on the interaction with auxiliary subunits, which are known to influence Ca^{2+} channel inactivation properties (38).

Ca^{2+} -dependent inactivation seems to be mediated directly by binding of Ca^{2+} ions to the channel (39). Elimination of the Ca^{2+} selectivity by the E1145Q mutation in the pore region of repeat III of rabbit cardiac α_{1C} was associated with a loss of Ca^{2+} -dependent inactivation (27). A Ca^{2+} binding site has also been implicated for a carboxyl-terminal segment near the transmembrane region IVS6 that includes a putative Ca^{2+} binding EF-hand motif (40–42). This motif is essential for Ca^{2+} -dependent inactivation, although additional residues downstream to the EF-domain are required to exhibit the full effect (42–45). On the other hand, neither truncation of up to 70% of the carboxyl-terminal tail of cloned α_{1C} subunits (15, 28) nor cytoplasmic modification by trypsin of cloned cardiac Ca^{2+} channels in HEK 293 cells (15) and endogenous Ca^{2+} channels in ventricular myocytes (35) had any effect on Ca^{2+} -dependent inactivation. However, in another study, Ca^{2+} -dependent inactivation in ventricular myocytes was abolished by trypsin digestion (46), indicating that there is a limit to the extent by which the carboxyl terminus can be shortened before inactivation

is impaired.

Our data show that substituting a stretch of 81 amino acids of $\alpha_{1C,86}$ for a segment of 80 amino acids in $\alpha_{1C,77}$ not only affects voltage-dependent inactivation, it also eliminates Ca^{2+} -dependent inactivation. This substitution left the four putative transmembrane domains and the EF-hand motif intact. These structural regions are identical in both α_{1C} constructs. Thus, our study supports recent observations (43–45) suggesting that the EF-hand motif is not the only determinant of Ca^{2+} -dependent inactivation (42). We could narrow down a carboxyl-terminal regulatory domain to a segment of maximally 81 amino acids.

Our studies have shown an alternatively spliced segment in the carboxyl terminus of the human α_{1C} subunit, which determines inactivation properties of the Ca^{2+} channel. It remains to be elucidated which parts and residues encoded by exons 40–42 are involved in voltage-dependent inactivation and whether these same sites are responsible for abolishing Ca^{2+} -dependent inactivation of $\alpha_{1C,86}$. Furthermore, it will be of great importance to clarify whether an $\alpha_{1C,86}$ -like splice variant is a functional class C Ca^{2+} channel in the brain.

Acknowledgments—We thank F. Hofmann (Munich) and V. Flockerzi (Heidelberg) for a gift of clones of β and $\alpha_2\delta$ subunits, J. Tytgat (Leuven) for providing pGEMHE, H. Porzig and K. Baltensperger for reading the manuscript, and H. Van Hees for excellent technical assistance.

REFERENCES

- Birnbaumer, L., Campell, K. P., Catterall, W. A., Harpold, M. M., Hofmann, F., Horne, W. A., Mori, Y., Schwartz, A., Snutch, T. P., Tanabe, T., and Tsien, R. W. (1994) *Neuron* **13**, 505–506
- Eckert, R., and Chad, J. E. (1984) *Prog. Biophys. Mol. Biol.* **44**, 215–267
- Regulla, S., Schneider, T., Nastainczyk, W., Meyer, H. E., and Hofmann, F. (1991) *EMBO J.* **10**, 45–49
- Catterall, W. A., and Striessnig, J. (1992) *Trends Pharmacol. Sci.* **13**, 256–262
- Tang, S., Yatani, A., Bahinski, A., Mori, Y., and Schwartz, A. (1993) *Neuron* **11**, 1013–1021
- Bangalore, R., Baidur, N., Rutledge, A., Triggle, D. J., and Kass, R. S. (1994) *Mol. Pharmacol.* **46**, 660–666
- Grabner, M., Wang, Z., Hering, S., Striessnig, J., and Glossmann, H. (1996) *Neuron* **16**, 207–218
- Catterall, W. A. (1991) *Science* **253**, 1499–1500
- Hofmann, F., Biel, M., and Flockerzi, V. (1994) *Annu. Rev. Neurosci.* **17**, 399–418
- Mikami, A., Imoto, K., Tanabe, T., Niidome, T., Mori, Y., Takeshima, H., Narumiya, S., and Numa, S. (1989) *Nature* **340**, 230–233
- Soldatov, N. M. (1994) *Genomics* **22**, 77–87
- Perez-Reyes, E., Wei, X., Castellano, A., and Birnbaumer, L. (1990) *J. Biol. Chem.* **265**, 20430–20436
- Soldatov, N. M. (1992) *Proc. Natl. Acad. Sci. U. S. A.* **89**, 4628–4632

14. Wei, X., Neely, A., Lacerda, A. E., Olcese, R., Stefani, E., Perez-Reyes, E., and Birnbaumer, L. (1994) *J. Biol. Chem.* **269**, 1635–1640
15. Klöckner, U., Mikala, G., Varadi, M., Varadi, G., and Schwartz, A. (1995) *J. Biol. Chem.* **270**, 17306–17310
16. Soldatov, N. M., Bouron, A., and Reuter, H. (1995) *J. Biol. Chem.* **270**, 10540–10543
17. Krieg, P. A., and Melton, D. A. (1984) *Nucleic Acids Res.* **12**, 7057–7070
18. Liman, E. R., Tytgat, J., and Hess, P. (1992) *Neuron* **9**, 861–871
19. Schuurman, R., and Keulen, W. (1991) *Biotechniques* **10**, 185
20. Bouron, A., Soldatov, N. M., and Reuter, H. (1995) *FEBS Lett.* **377**, 159–162
21. Singer, D., Biel, M., Lotan, I., Flockerzi, V., Hofmann, F., and Dascal, N. (1991) *Science* **253**, 1553–1557
22. Ruth, P., Röhrkasten, A., Biel, M., Bosse, E., Regulla, S., Meyer, H. E., Flockerzi, V., and Hofmann, F. (1989) *Science* **245**, 1115–1118
23. Mori, Y., Friedrich, T., Kim, M., Mikami, A., Nakai, J., Ruth, P., Bosse, E., Hofmann, F., Flockerzi, V., Furuchi, T., Mikoshiba, K., Imoto, K., Tanabe, T., and Numa, S. (1991) *Nature* **350**, 398–402
24. Hullin, R., Singer-Lahat, D., Freichel, M., Biel, M., Dascal, N., Hofmann, F., and Flockerzi, V. (1992) *EMBO J.* **11**, 885–890
25. Ellinor, P. T., Yang, J., Sather, W. A., Zhang, J. F., and Tsien, R. W. (1995) *Neuron* **15**, 1121–1132
26. Neely, A., Olcese, R., Wei, X., Birnbaumer, L., and Stefani, E. (1994) *Biophys. J.* **66**, 1895–1903
27. Zong, S., Zhou, J., and Tanabe, T. (1994) *Biochem. Biophys. Res. Commun.* **201**, 1117–1123
28. Zong, X. G., and Hofmann, F. (1996) *FEBS Lett.* **378**, 121–125
29. Hille, B. (1992) *Ionic Channels of Excitable Membranes*, pp. 1–19, Sinauer Associates, Sunderland
30. McDonald, T. F., Pelzer, S., Trautwein, W., and Pelzer, D. J. (1994) *Physiol. Rev.* **74**, 365–507
31. Welling, A., Kwan, Y. W., Bosse, E., Flockerzi, V., Hofmann, F., and Kass, R. S. (1993) *Circ. Res.* **73**, 974–980
32. Parent, L., and Gopalakrishnan, M. (1995) *Biophys. J.* **69**, 1801–1813
33. Zhang, J., Ellinor, P. T., Aldrich, R. W., and Tsien, R. W. (1994) *Nature* **372**, 97–100
34. Yatani, A., Bahinski, A., Wakamori, M., Tang, S., Mori, Y., Kobayashi, T., and Schwartz, A. (1994) *Mol. Cell. Biochem.* **140**, 93–102
35. Schmid, R., Seydl, K., Baumgartner, W., Groschner, K., and Romanin, C. (1995) *Biophys. J.* **69**, 1847–1857
36. Catterall, W. A. (1995) *Annu. Rev. Biochem.* **64**, 493–531
37. Yang, N. B., George, A. L., and Horn, R. (1996) *Neuron* **16**, 113–122
38. Isom, L. L., De-Jongh, K. S., and Catterall, W. A. (1994) *Neuron* **12**, 1183–1194
39. Imredy, J. P., and Yue, D. T. (1994) *Neuron* **12**, 1301–1318
40. Babitch, J. (1990) *Nature* **346**, 321–322
41. Tsien, R. W., Ellinor, P. T., and Horne, W. A. (1991) *Trends Pharmacol. Sci.* **12**, 349–354
42. DeLeon, M., Wang, Y., Jones, L., Perez-Reyes, E., Wei, X. Y., Soong, T. W., Snutch, T. P., and Yue, D. T. (1995) *Science* **270**, 1502–1506
43. Wang, Y., DeLeon, M., and Yue, D. T. (1996) *Biophys. J.* **70**, A238
44. Olcese, R., Zhou, J., Qim, N., Birnbaumer, L., and Stefani, E. (1996) *Biophys. J.* **70**, A186
45. Adams, B., and Tanabe, T. (1996) *Biophys. J.* **70**, A238
46. You, Y. D., Pelzer, D. J., and Pelzer, S. (1995) *Biophys. J.* **69**, 1838–1846